Int. J. Electrochem. Sci., 15 **(2020)** 4089 – 4101, doi: 10.20964/2020.05.60

International Journal of
ELECTROCHEMICAL
SCIENCE
www.electrochemsci.org

Application of EIS and transmission line model to study the effect of arrangement of graphene on electromagnetic shielding and cathodic protection performance of zinc-rich waterborne epoxy coatings

Xiao Wang[1,3,#], *Jing Lv*[2,#], *Rui Ding*[2,*], *Tai-jiang Gui*[1], *Ming-Liang Sun*[1]

[1] Ocean University of China, Qingdao 266071, China;
[2] College of Oceanology, Yantai University, Yantai, 264005, China;
[3] Marine Chemical Research Institute, State Key Laboratory of Marine Coatings, Qingdao 266071, China;
# These authors contributed equally to this work.
[*]E-mail: dingrui@ytu.edu.cn

Received: 1 Janaury 2020 / *Accepted:* 10 February 2020 / *Published:* 10 April 2020

In this paper, polyol solvothermal method was applied to prepare magnetic graphene (Fe_3O_4@G), with the utilization of $FeCl_3$ as the iron source. The waterborne zinc-rich epoxy coatings without Fe_3O_4@G, and with unoriented Fe_3O_4@G or oriented Fe_3O_4@G were produced, and the arrangement of Fe_3O_4@G on the shielding and cathodic protection performance of the coatings were studied. Ordered by uniform strong magnetic field, the shielding performance of the oriented distribution array of Fe_3O_4@G was significantly improved because of the arrangement parallel to the surface of the metal substrate. On the other side, compared to disordered random distribution, the ordered and aligned arrangement of Fe_3O_4@G impaired the cathodic protection performance of zinc-rich coatings, and this was related to the reduction of electron conduction channels in the coatings.

Keywords: Magnetic graphene, Cathodic protection, Shielding protection, Zinc-rich coatings

1. INTRODUCTION

Corrosion caused by the contact of metal materials with oxygen, chloride ions and water was the main reason for the failure of metal materials [1-3]. Cathodic protection coatings were commonly used primers in anti-corrosion coating systems [4, 5]. In cathodic protection coatings, more active metals such as zinc and aluminum were introduced [6]. The galvanic interaction between them and the relatively inert metal matrix was utilized to generate electrochemical protection for the metal matrix [7, 8]. Zinc-rich coatings were cathodic protection primers with a very wide range of applications [9]. The active

zinc formed corrosion couples with the steel substrate. The former acted as the sacrificial anode with a low corrosion potential, and the latter acted as the cathode. The mixing potential of the galvanic systems was much lower than the corrosion potential of iron. However, the application of zinc-rich coatings was plagued by its shortcomings. In zinc-rich coatings, effective electrical contact between zinc particles and between zinc particles and the metal substrate was the prerequisite for cathodic protection. Generally, very high zinc content, up to 80-90 wt%, was present in zinc-rich coatings. This significantly created large number of pinholes and gaps in the coatings and damaged the barrier to corrosive media. The introduction of conductive or optoelectronic materials was used to replace part of the zinc powder to build additional conductive channels, thereby reducing the amount of zinc and the pore defects of the coatings. The former included carbon black [10-13], graphite [14], carbon nanotubes, and the latter included nano-Ti_2O and et al [9, 15, 16]. On the other hand, the introduction of lamellae or nano-fillers directly improved the shielding properties of coatings by establishing shielding layers or filling pore defects, such as mica iron oxide [17] and nano-montmorillonite [18]. Although these studies achieved some improvements in zinc-rich coatings, their shielding effects and cathodic protection generally did not improve simultaneously. Graphene possessed ultra-thin monoatomic layer structure, large specific surface area, and excellent electronic conductivity[19-21]. In theory, graphene could promote both types of protective effects of zinc-rich coatings. However, in our previous research [22-24] and the literatures [25, 26], it was found that there were some difficulties and obstacles in the application of graphene to zinc-rich coatings. First, the higher the oxidation degree of graphene, the more structural defects, the worse the shielding properties, and the worse its conductivity. Due to the lack of active sites, it was difficult for reduced graphene to achieve good dispersion through modification of dispersant groups [27]. Secondly, the non-oriented arrangement of graphene in the coatings did not fully exert its shielding performance. In theory, the arrangement that was most beneficial to the barrier properties of the coatings was ordered arrangement parallel to the metal substrate. In this paper, reduced graphene loaded with magnetic Fe_3O_4 nanoparticles was prepared. The steric hindrance of ferric oxide nanoparticles inhibited the agglomeration of graphene. This not only guaranteed the conductivity and dispersion effect of the reduced graphene, but also achieved its directional arrangement in uniform magnetic field. The paper also further studied the effect of its orientation on the shielding and cathodic protection of zinc-rich coatings.

2. EXPERIMENTAL METHODS

In the preparation of magnetic graphene (Fe_3O_4@G), the $FeCl_3$ was iron source. Propylene glycol, the solvent was reducing agent in solvothermal method. In 200 mL of propylene glycol, 1.0 g of graphene was dispersed by 2.0 hours of ultrasonic treatment. And graphene suspension was obtained. After addition of 1.3 g of $FeCl_3$ and 0.5 hour of ultrasonic treatment, 4.2 g of CH_3COONa was put in the suspension and additional 0.5 hour of ultrasound processing was carried out. Then the suspension was transferred into a polytetrafluoroethylene reactor which was placed in a vacuum drying oven and heated for 12 hours at 195 ℃. After that, centrifugation was implemented, and the precipitate was taken out and

washed repeatedly with deionized water. After 12 hours of drying in environment of 60 ℃, magnetic Fe_3O_4@G was obtained.

The waterborne epoxy resin and the curing agent 8570 were purchased from Momentive Advanced Materials Group Ltd (USA) respectively. The Fe_3O_4@G-Zn mixed dispersion solution was composed of magnetic graphene, nano zinc powder and suitable solvent. The mass ratio of Fe_3O_4@G and nano zinc powder was 1:99. Distilled water and waterborne epoxy resin were mixed at the mass ratio of 1:5 and stirred vigorously. Then 60 wt% of Fe_3O_4@G-Zn mixed dispersion solution was added into the waterborne epoxy resin. Continuous vigorous agitation was performed to ensure adequate and even mixing of the components. After introducing 25 wt% of curing agents, the coatings with thickness of 30μm were sprayed on the surface of Q235 steel. The orientation of Fe_3O_4@G was achieved by a uniform magnetic field generated by two NdFeB magnets during the curing process of the coatings.

In the analysis and testing experiments of materials, the following instruments were used: Quanta 200 scanning electron microscope (Thermo Fisher Scientific, USA), HF-3300 field emission transmission electron microscope (Hitachi, Japan), Q50 thermal gravimetric analyzer (TA Instruments, USA), D8 Advance X-ray diffractometer (Bruker, Germany), MPMS-7XL magnetic property measurement system (Quantum Design, USA), AutoLab PGSTAT 302N electrochemical workstation (Metrohm. Inc. Switzerland). The electrochemical impedance spectroscopy was measured using the three-electrode system, in which saturated calomel electrode was reference electrode and platinum mesh electrode was auxiliary electrode. The measurement of the cathodic current followed the methods in the literature [22].

3. RESULTS AND DISCUSSION

3.1 Characterization of magnetic graphene

Comparing the TEM images of graphene and Fe_3O_4@G (figure 1a and 1b), it was found that graphene was flaky, and spherical ferric oxide nanoparticles with the diameter of about 20~30 nm were supported on the graphene surface. As a whole, the distribution of Fe_3O_4 nanoparticles was relatively uniform, and there were local differences in compactness and sparseness. The inset in figure 1 (b) illustrated that Fe_3O_4@G exhibited sensitive and significant response to the magnet.

XRD analysis was shown in figure 1(c). Graphene exhibited a typical diffraction peak representing (002) crystal plane at around 23˚ [28]. The diffraction peak was wide due to the decrease in crystal structural integrity and increase in disorder. In addition, the splitting of the peak indicated that there were certain defects in the crystal structure of graphene [29]. XRD images of Fe_3O_4@G exhibited multiple diffraction peaks of Fe_3O_4 nanocrystals at 2θ of 31.5˚, 36.7˚, 44.1˚, 54.0˚, 57.8˚ and 63.1˚, which corresponded to crystal planes of (220), (311), (400), (422), (511) and (440), respectively. This matched the JCPDS card of Fe_3O_4.

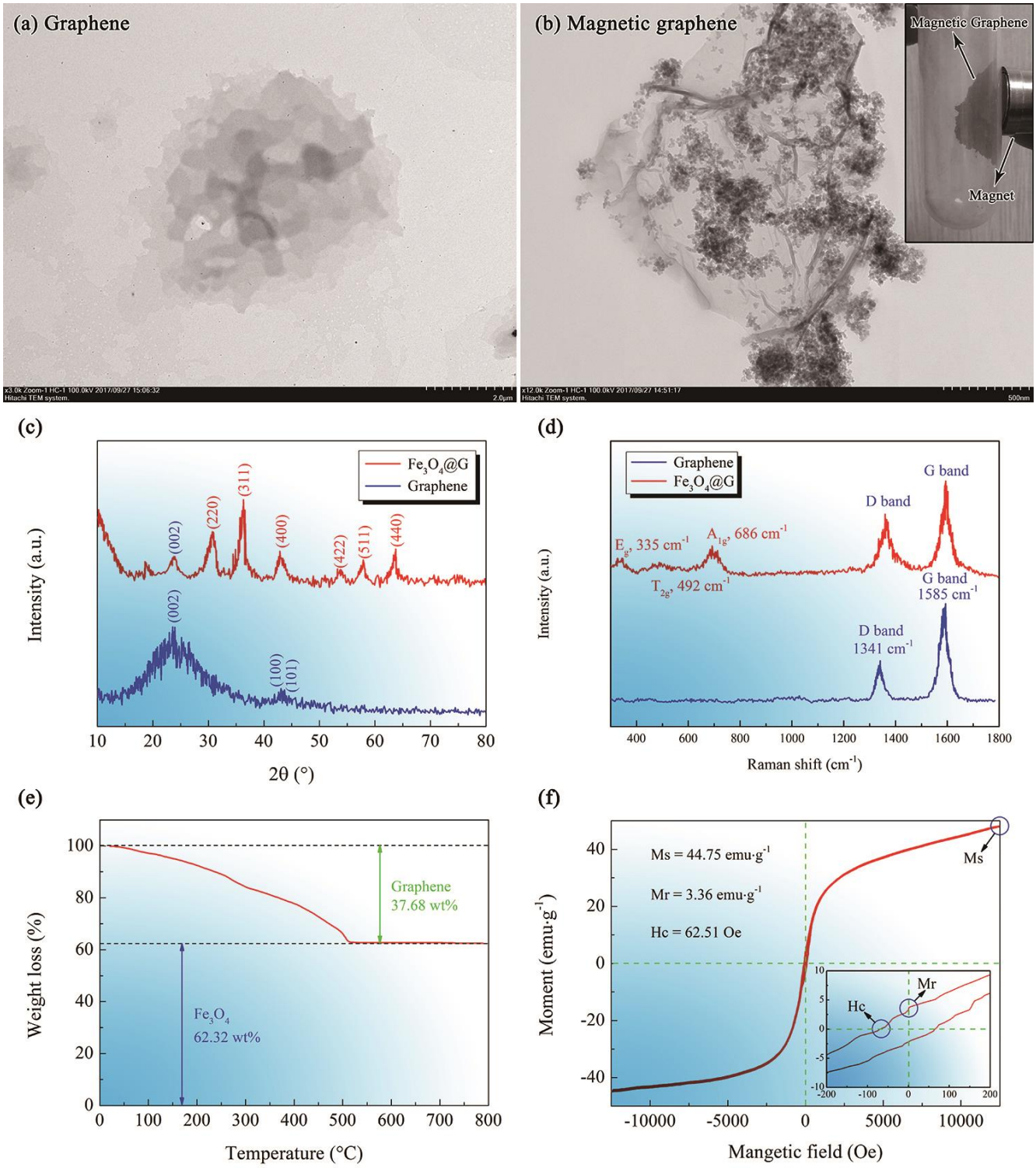

Figure 1. Analysis results of graphene and Fe_3O_4@G: (a) TEM of graphene, (b) TEM of Fe_3O_4@G (inside illustration showed the response of Fe_3O_4@G to magnet), (c) XRD and (d) Raman Spectrum of graphene and Fe_3O_4@G, (e) thermogravimetric analysis, (f) hysteresis loop

Figure 1 (d) was the Raman spectrum of graphene and Fe_3O_4@G. The main characteristic peak (G peak) of graphene was caused by in-plane vibration of carbon atoms, and appeared near 1585 cm^{-1}. The G peak was broad due to the stacking of graphene sheets. The more the graphene layers, the wider the G peak. The D peak between 1270 and 1450 cm^{-1} was disordered vibration peak of graphene. The

intensity ratio of the D peak to the G peak (I_D/I_G) of graphene was about 0.52, and that of Fe_3O_4@G was about 0.77. The value of I_D/I_G was inversely proportional to the average size of graphene crystallites. This showed that the average size of the graphene crystallites was reduced after the magnetization by the solvothermal methods. In the Raman spectrum of Fe_3O_4@G, the characteristic peaks of Fe_3O_4 also appeared. The peaks around 335 cm^{-1} and 492 cm^{-1} were E_g and T_{2g} symmetrical modes of Fe_3O_4. The peak near 686 cm^{-1} was the A_{1g} vibration mode of Fe_3O_4.

Figure 1(e) showed the thermogravimetric curve of Fe_3O_4@G. As the temperature increased, the carbon atoms in graphene were gradually oxidized to gas, resulting in the decrease in the thermogravimetric curve. When graphene was completely oxidized and oxides of iron remained, the thermogravimetric curve appeared horizontal. Thermogravimetric analysis shown that the mass fraction of graphene composed of carbon in Fe_3O_4@G was about 37.68 wt% and the mass fraction of Fe_3O_4 was about 62.32 wt%. This indicates that Fe_3O_4 nanoparticles were supported on the surface of graphene, and Fe_3O_4@G was successfully synthesized.

The hysteresis loop of Fe_3O_4@G was shown in figure 1(f). It showed the relationship between the magnetization M and the magnetic field H during repeated magnetization of magnetic substance. Due to the influence of non-magnetic graphene, the saturation magnetization M_s of Fe_3O_4@G was lower than that of Fe_3O_4 nanoparticles (above 60 $emu \cdot g^{-1}$), and was about 44.75 $emu \cdot g^{-1}$. The remanence M_r and coercive force H_c of Fe_3O_4@G were obtained from the partially enlarged view, and they were M_r = 3.36 $emu \cdot g^{-1}$ and H_c = 62.51 Oe. The small remanence and coercive force indicated that the Fe_3O_4@G was weakly magnetized, which reduced the risk of Fe_3O_4@G agglomeration under its own magnetic effect.

3.2 Effect of arrangement of Fe_3O_4@G on cathodic protection performance of zinc-rich coatings

In this section, the effects of magnetic graphene and its alignment on the cathodic protection performance of waterborne zinc-rich coatings were investigated by electrochemical methods. Figures 2(a) and(b) were Nyquist and Bode plots of the electrochemical impedance spectroscopy of the three coatings immersed in 3.5 wt% NaCl solution for 24 hours. Because the zinc-rich coatings were conductive, the anti-corrosion performance the coatings could not be judged simply by the impedance value [30]. In the literature, graphene was applied to zinc-rich coatings, and the presence of graphene significantly reduced the overall impedance of zinc-rich coatings. However, this did not mean that the anti-corrosion performance of the coatings was weakened, because the zinc-rich coatings did not achieve corrosion protection with the simple shielding effect [26]. In-depth and detailed analysis and fitting were performed. The Nyquist diagram in Figure 2(a) showed that the capacitance arcs of zinc-rich coatings with Fe_3O_4@G were smaller than that of the zinc-rich coatings without Fe_3O_4@G, and the orientational arrangement of Fe_3O_4@G increased the capacitive arcs. This was because the conductive Fe_3O_4@G reduced the resistance of the coatings, and at the same time caused the capacitance between the inner and outer surfaces of the coatings to leak [22], thereby reducing the overall impedance of the coating system. After Fe_3O_4@G was aligned parallel to the metal surface, the effective contact between graphene

nanosheets and between Fe_3O_4@G and zinc powder was reduced, so the overall impedance of the coating system was increased.

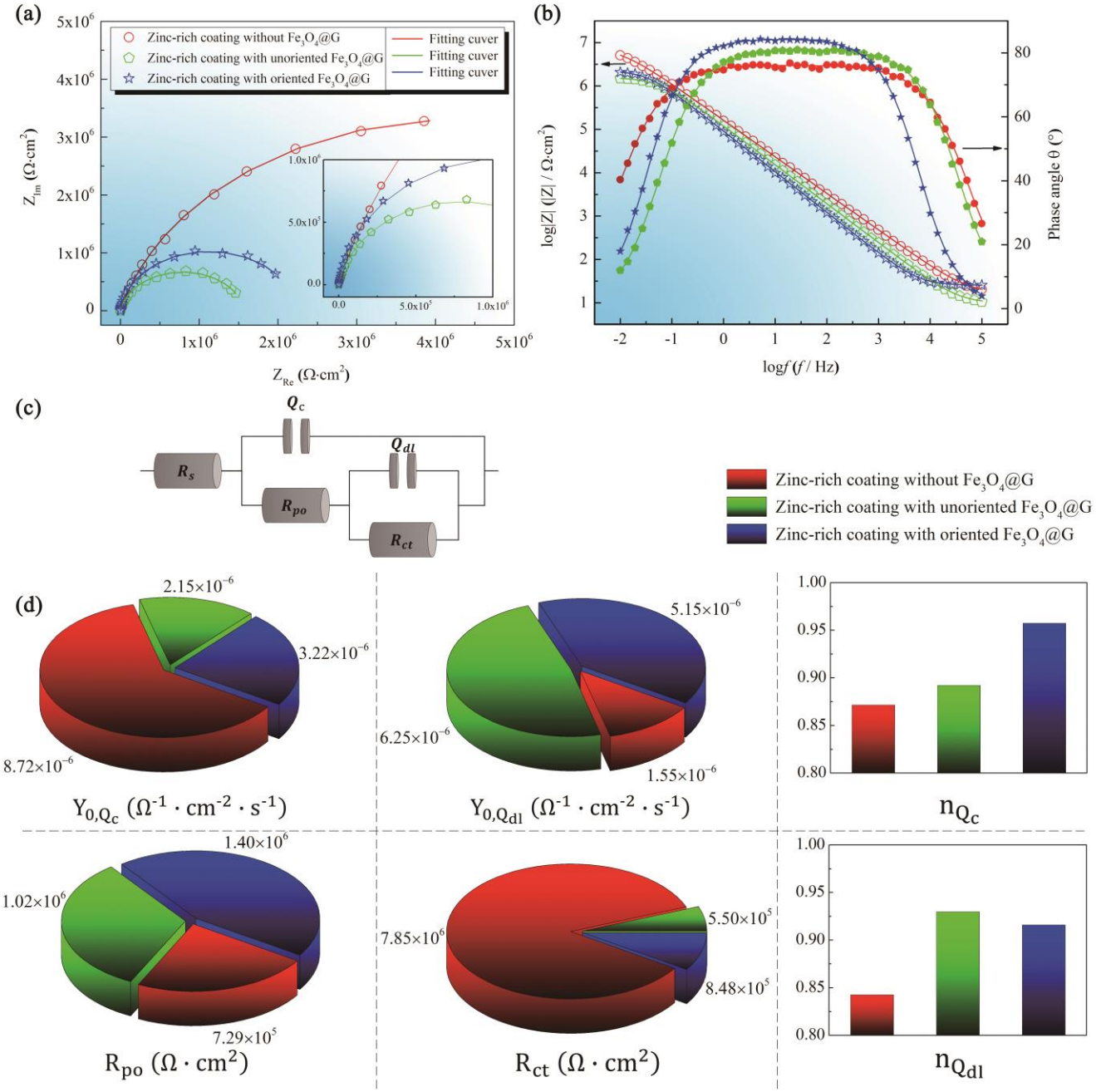

Figure 2. The (a) Nyquist plots and (b) Bode plots of electrochemical impedance spectroscopy of the three kinds of coatings, (c) equivalent circuit for the fitting processes and (d) the fitting results

For zinc-rich coatings with unoriented Fe_3O_4@G, two capacitance arcs appeared in the Nyquist diagram, and accordingly two peaks were presented in the Bode-phase angle diagram. For zinc-rich coatings without Fe_3O_4@G and with oriented Fe_3O_4@G, although the Nyquist diagram showed one capacitance arc and the Bode-phase angle diagram showed one peak, the application of equivalent circuit containing one parallel structure of resistor and capacitor did not obtained satisfactory fitting results. The equivalent circuit in figure 2(c), which included two parallel structure of resistors and capacitors,

fitted the electrochemical impedance spectroscopy of each coating well. This was because the two time-constants reflecting the dielectric process of the coatings and the electrochemical reaction process of zinc were close, resulting in similar radii of the two capacitance arcs in the Nyquist diagram and one peak in the Bode-phase angle diagram accordingly [31]. In the equivalent circuit of figure 2(c), R_s was the solution resistance, R_{po} was the coating micropore resistance, Q_c was the coating capacitance, R_{ct} was the charge transfer resistance during the electrochemical corrosion of zinc, and Q_{dl} was the double layer capacitance on the surface of zinc particles.

The fitting results were shown in figure 2(d). For the dielectric process of the coatings, the addition of Fe_3O_4@G significantly reduced the admittance coefficient $Y_{0,Qc}$ of the coating capacitance and increased the coating micropore resistance R_{po}. The coating micropore resistance reflected the ability of coatings to block the penetration of corrosive media, and the two were positively correlated [32]. The admittance coefficient reflected the capacitive capacity of the coatings to a certain extent [33], which explained the capacitance leakage caused by conductive Fe_3O_4@G. The horizontal orientation of Fe_3O_4@G made the permeation path of corrosive medium tortuous, reflecting the enhanced shielding performance of the coatings. Meanwhile, the horizontal orientation of Fe_3O_4@G reduced the number of electron conduction channels in the vertical direction. This weakened the capacitance leakage effect, and the admittance coefficient of the coating capacitance was increased. For the electrochemical corrosion of zinc powder, the addition of Fe_3O_4@G significantly increased the admittance coefficient of the double layer capacitance $Y_{0,Qdl}$ and reduced the charge transfer resistance R_{ct}. The increase in the admittance coefficient reflected the enlargement in the double layer capacitance [34], which in turn explained the raise in the activation rate of zinc powder surface. The decrease of the charge transfer resistance indicated that the resistance of the electrochemical reaction of zinc was weakened. After Fe_3O_4@G was aligned horizontally, as the electron conduction channels were reduced compared with the case of non-aligned alignment, the admittance coefficient of the double layer capacitance was reduced, and the charge transfer resistance was increased. This reflected the decrease in the surface of the active zinc powder and the increase in the electrochemical reaction resistance, indicating that the ordered arrangement of Fe_3O_4@G was not conducive to the anode sacrifice of zinc and the cathodic protection on iron matrix. The literature also showed that graphene enhanced the anode sacrificial corrosion of zinc powder, and this promotion was more obvious than Fe_3O_4@G [26]. After graphene was modified by conductive polyaniline fibers, the promotion effect was further enhanced [25]. This indicated that the preparation of Fe_3O_4@G for the directional alignment was not conducive to the cathodic protection of zinc-rich coatings due to the increase in the size of the Fe_3O_4@G and the horizontal orderly arrangement. The dispersion coefficient n represented the degree to which the capacitor element deviated from the ideal capacitor [35], and to some extent reflected the uniformity of the coatings or the uniformity of activation of zinc powder. The addition of Fe_3O_4@G and its ordered arrangement increased the dispersion coefficient of the coating capacitance n_{Qc} and enhanced the uniformity of the coatings. Obtained from the dispersion coefficient of the electric double layer capacitance n_{Qdl}, Fe_3O_4@G also made the activation of zinc powder more uniform, but the orientation weakened this effect.

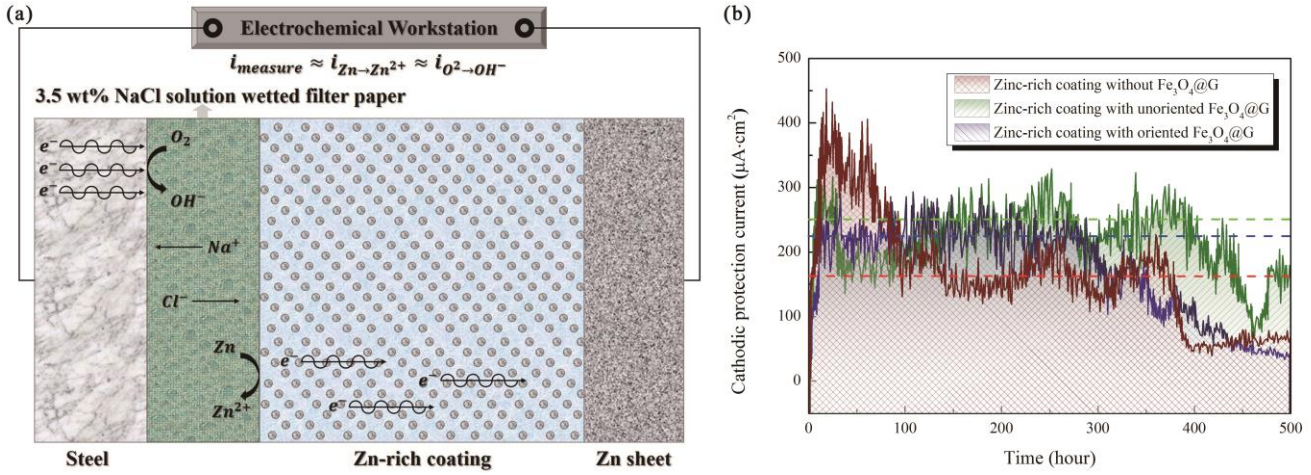

Figure 3. Measuring principle of cathodic protection current and the cathodic protection current curves of the three kinds of coatings

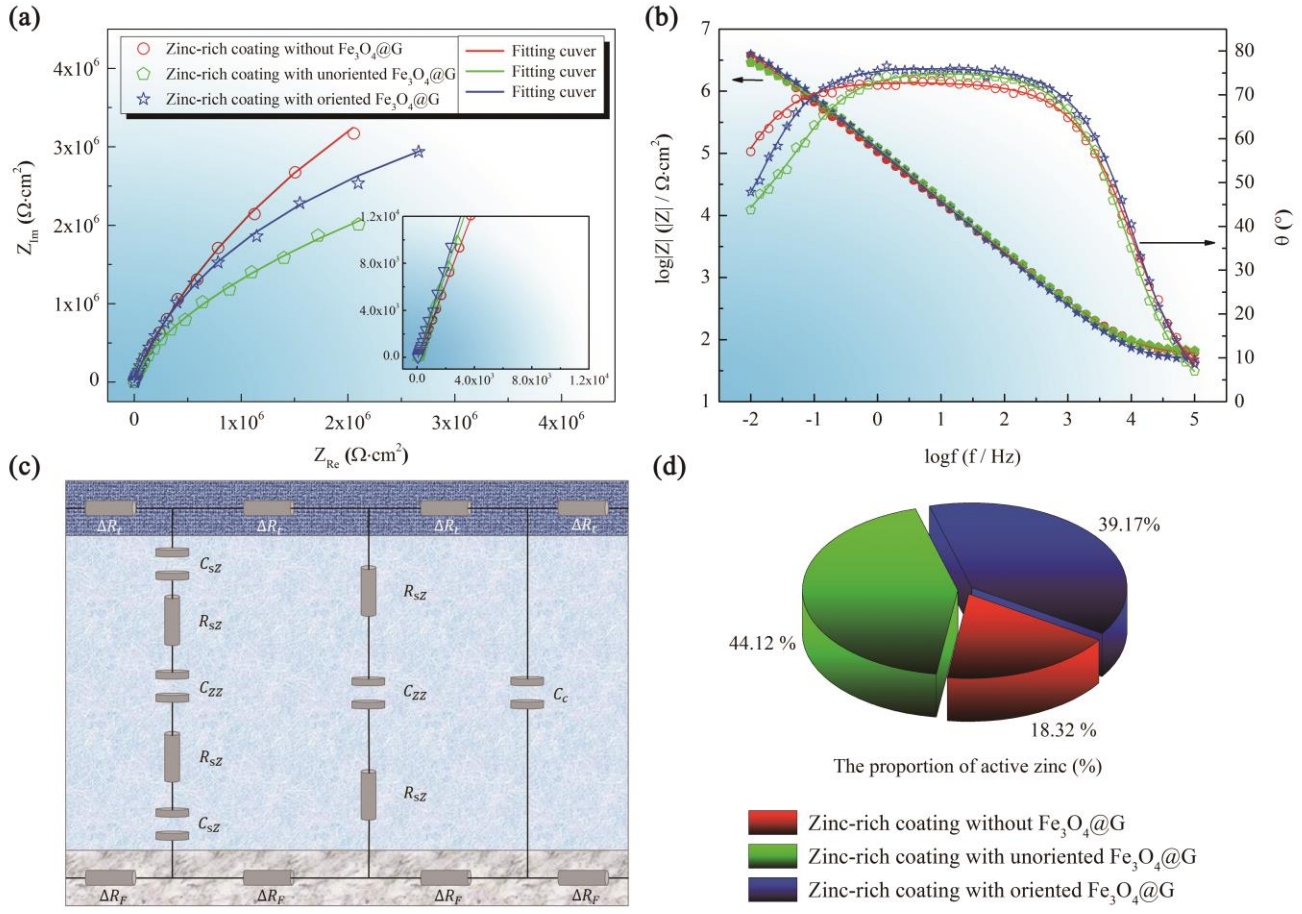

Figure 4. The (a) Nyquist and (b) Bode plots of electrochemical impedance spectroscopy of three kinds of dry coatings that were not immersed in 3.5 wt% NaCl solution, (c) the transmission line model for the fitting of electrochemical impedance spectroscopy and (d) the proportion of active zinc particles in the three coatings

Based on the methods in the literatures [24] and [36] and principles shown in figure 3(a), the cathodic protection current of zinc powder in the coatings on steel substrate was measured and shown in figure 3(b). The effect of Fe_3O_4@G and its directional arrangement on the cathodic protection of zinc-rich coatings was observed more directly through the cathodic protection current curves. The presence of Fe_3O_4@G significantly increased the cathodic protection current density and prolonged the duration of cathodic protection. After orientation of Fe_3O_4@G, the promotion of cathodic protection was weakened in both current density and protection time. However, compared with the graphene zinc-rich coatings in the literature [22], the cathodic protection current of the zinc-rich coatings with Fe_3O_4 was significantly smaller than the former, which also reflected the increase in the size of graphene materials caused by the loading of ferric oxide greatly reduced the improvement effect on the cathodic protection of zinc-rich coatings.

The three dry coatings that was not immersed in 3.5 wt% NaCl solution was coated with conductive tape and subjected to electrochemical impedance spectroscopy [22]. By establishing the transmission line model of the dry coatings and fitting the electrochemical impedance spectroscopy, the influence principle of the addition and orientation of Fe_3O_4@G on the cathodic protection micro-mechanism of zinc-rich coatings was studied, that is, the changes of electrochemical structure inside the zinc-rich coatings. Figures 4 (a) and (b) were Nyquist and Bode plots of the electrochemical impedance spectroscopy of the three dry coatings that are not immersed in 3.5 wt% NaCl solution. The law was similar to the electrochemical impedance spectroscopy of the immersed coatings. The addition of conductive Fe_3O_4@G reduced the impedance, while the horizontal alignment weakened the conduction effect and increased the impedance slightly. In the Bode diagram, each phase angle curve showed one broad peak. There were two reasons for broad peaks. The first reason was that there was one parallel structure of resistor and capacitor in the equivalent circuit, and the resistance was very large and the capacitance was very small. The second reason was that there were multiple parallel structures of resistors and capacitors in the equivalent circuit, and the time constants of the parallel structures were similar, which caused the peaks of phase angle to merge into a broad one. In this paper, the three zinc-rich coatings were conductive coatings and possessed low electrical resistance, so the reason should be the second one. Based on this, the zinc particles in the coatings were divided into active and inactive ones [11], and corresponding transmission line model was established in figure 4(c). The former formed the RCR conductive branches, and the latter formed the CRCRC conductive branches. The proportions of the two branches were α and β, and $\alpha+\beta=1$ [10, 37]. In the studies of Marchebois [12, 37] and Meroufel [10], it was found that when the zinc powder content was higher, the proportion of activated zinc particles α decreased due to that the number of zinc particles distributed inside the coating increased significantly faster than the zinc particles contacted the coating interface. The ratio of active zinc branches α was obtained by fitting electrochemical impedance spectroscopy with transmission line model and shown in figure 4(d). The Zinc-rich coatings without Fe_3O_4@G possessed the lowest active zinc content. After adding Fe_3O_4@G, the content of active zinc increased significantly, and the orientation of Fe_3O_4@G caused the loss of activation of zinc powder. The reason was that the random and non-directional distribution of Fe_3O_4@G maximized the effective electrical contact between zinc particles. After the Fe_3O_4@G was aligned horizontally, although the electrical contact between zinc particles at the same level was guaranteed, the electrical contact between zinc particles located at different depths was

weakened. In the graphene zinc-rich coatings prepared in the literature [22], the increase effect of graphene on the proportion of active zinc particles was more significant than that of Fe_3O_4@G. This could also be explained by the larger size of Fe_3O_4@G.

3.3 Effect of arrangement of Fe_3O_4@G on shielding performance of zinc-rich coatings

The effect of the orientation of Fe_3O_4@G on the shielding properties of zinc-rich coatings was evaluated by the diffusion rate of water in the coatings. The moisture content of the coatings possessed clear quantitative relationship with the coating capacitance. Therefore, this paper investigated the time course of coating capacitance to study the diffusion process of water in the coatings, and then judged the effect of the orientation of Fe_3O_4@G on this process.

The coating capacitance was expressed as

$$C_c(t) = \varepsilon(t)\varepsilon_0 \frac{S}{L} \quad (1)$$

Where S was the coating area, L was the coating thickness, and ε_0 was the vacuum dielectric constant. Since the relative dielectric constant $\varepsilon(t)$ of the coating was

$$\varepsilon(t) = \varepsilon_d \times \varepsilon_w^{\upsilon(t)} \quad (2)$$

Where ε_d was relative dielectric constant of dry coatings, ε_w was relative dielectric constant of water, and $\upsilon(t)$ was the volume fraction of water in the coatings. It was obtained that

$$\upsilon(t) = \frac{\ln \frac{C_c(t)}{C_d}}{\ln \varepsilon_w} \quad (3)$$

Where C_d was the coating capacitance of the dry coatings, that is, the coating capacitance at $t = 0$. Let υ_∞ represented the volume fraction of water when the coatings were water-saturated [38], then

$$\frac{\ln C_c(t) - \ln C_d}{\ln C_\infty - \ln C_d} = \frac{\upsilon(t)}{\upsilon_\infty} \quad (4)$$

The total water content M(t) of the coatings (in $\mu g \cdot cm^2$) was calculated by the following formula [39]:

$$M(t) = SL\rho_w \upsilon(t) \quad (5)$$

According to J. Crank's research, there was an approximate relationship between the total water content and the saturated water content of the coatings [22]:

$$\frac{\ln C_c(t) - \ln C_d}{\ln C_\infty - \ln C_d} = \frac{M(t)}{M_\infty} \quad (6)$$

Therefore, the diffusion coefficient D of water in the coatings was [40]:

$$\sqrt{D} = \frac{L\sqrt{\pi}}{2(\ln C_\infty - \ln C_d)} \frac{d\ln C_c}{d\sqrt{t}} \quad (7)$$

Where $dlnC_c/d\sqrt{t}$ was the slope of the coating capacitance curves.

Figure 5(a~c) illustrated that the natural logarithm of the coating capacitance possessed approximately linear relationship with the square root of time. This was the characteristic of Fick diffusion, so the application of the above equations was feasible. When Fe_3O_4@G was added, the slope decreased. The horizontal orientation of Fe_3O_4@G further reduced the slope. This reflected the slowdown in the diffusion process. Calculated by equation (7), the diffusion coefficient D of water in

each coating was obtained and shown in figure 5(d). Consistent with the slopes, the D of the zinc-rich coatings without Fe_3O_4@G was the largest, and the D of the zinc-rich coatings with oriented Fe_3O_4@G was the smallest. The measurement and calculation of the water diffusion coefficient confirmed that the oriented arrangement of Fe_3O_4@G improved the shielding performance of zinc-rich coatings.

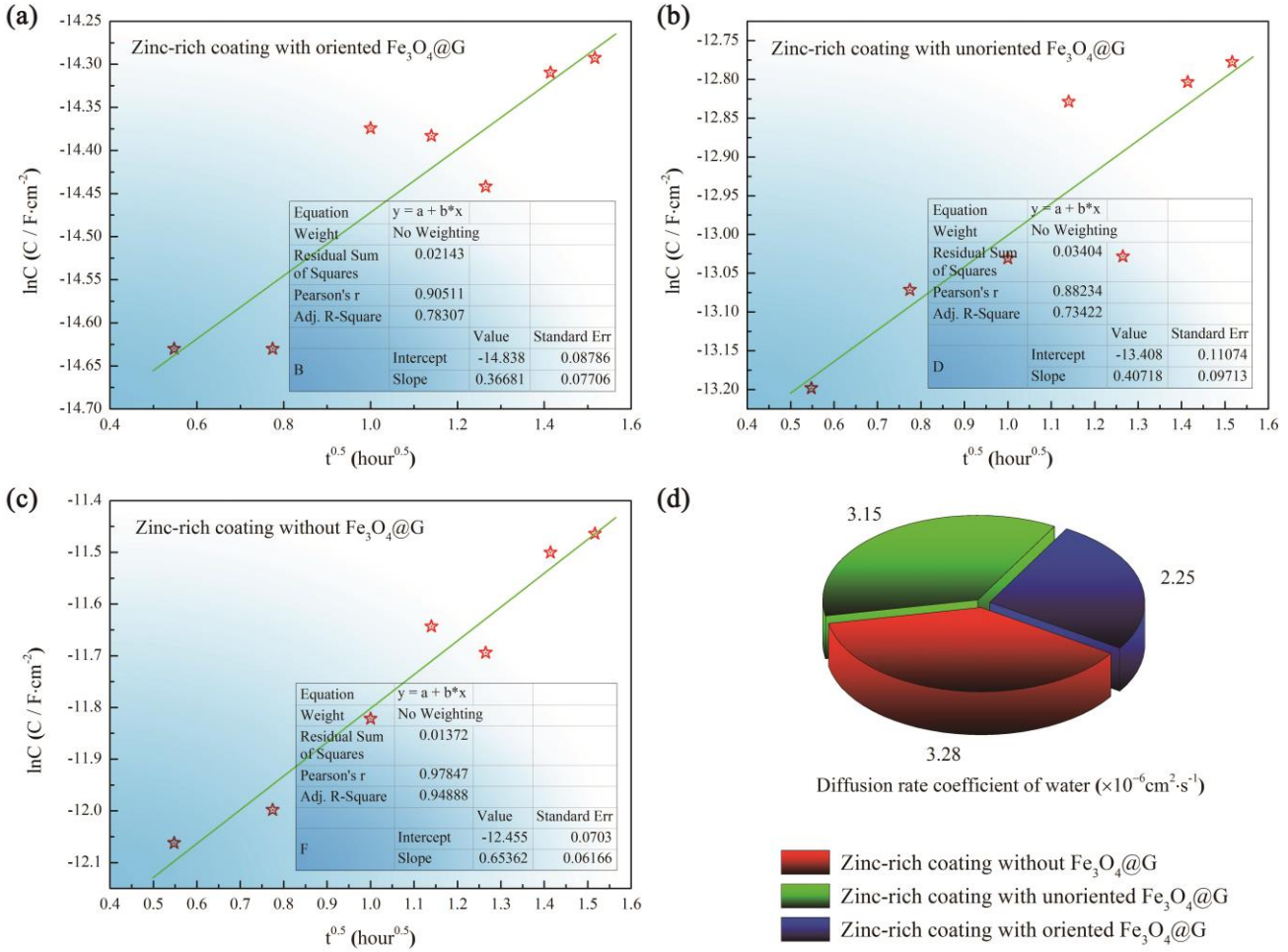

Figure 5. Curves of coating capacitance of the (a) zinc-rich coatings with oriented Fe_3O_4@G, (b) zinc-rich coatings with unoriented Fe_3O_4@G, (c) zinc-rich coatings without Fe_3O_4@G, and the diffusion coefficient of water in the three kinds of coatings

4. CONCLUSION

Magnetic graphene Fe_3O_4@G with obvious response to magnetic field was prepared and applied in zinc-rich coatings. XRD and Raman spectroscopy indicated that magnetic Fe_3O_4 was supported on the surface of graphene. Fe_3O_4@G exhibited small remanence and coercive force, which reduced the risk of agglomeration of Fe_3O_4@G under its own magnetic field. Compared to the non-oriented distribution, the directional arrangement of Fe_3O_4@G parallel to the metal substrate weakened the electron conduction in the vertical direction, and therefore was not conducive to the improvement of the cathodic protection performance. Through the fitting and analysis of the transmission line model, this phenomenon was explained from the micro perspective, that was, the orientation of Fe_3O_4@G reduced

the proportion of active zinc by reducing the vertical electron transport channels. However, this orientation significantly reduced the rate of diffusion and penetration of corrosive media in zinc-rich coatings.

ACKNOWLEDGEMENTS
We gratefully acknowledge the financial support from Open Research Fund of State Key Laboratory for Marine Coatings, Grand NO. 20190601DR.

References

1. H. Tian, X. Zhang and Y. Bu, *ACS Sustain. Chem. Eng.*, 6 (2018) 7346.
2. M.A. Hou-Yi, C.Y. Cui and T. Chen, *Electrochem.*, 17 (2011) 288.
3. A.A. Nazeer and M. Madkour, *J. Mol. Liq.*, 253 (2018) 11.
4. B. Ramezanzadeh, G. Bahlakeh, M.H. Mohamadzadeh Moghadam and R. Miraftab, *Chem. Eng. J.*, 335 (2018) 737.
5. Y. Hayatgheib, B. Ramezanzadeh, P. Kardar and M. Mahdavian, *Corr. Sci.*, 133 (2018) 358.
6. W. Sun, L. Wang, T. Wu, Y. Pan and G. Liu, *J. Mater. Chem. A*, 3 (2015) 16843.
7. S. Pourhashem, M.R. Vaezi, A. Rashidi and M.R. Bagherzadeh, *Prog. Org. Coat.*, 111 (2017) 47.
8. J. Li, Q. Feng, J. Cui, Q. Yuan, H. Qiu, S. Gao and J. Yang, *Comp. Sci. Technol.* 151 (2017) 282.
9. Y. Cubides and H. Castaneda, *Corr. Sci.*, 109 (2016) 145.
10. A. Meroufel and S. Touzain, *Prog. Org. Coat.*, 59 (2007) 197.
11. H. Marchebois, C. Savall, J. Bernard and S. Touzain, *Electrochim. Acta*, 49 (2004) 2945.
12. H. Marchebois, S. Touzain, S. Joiret, J. Bernard and C. Savall, *Prog. Org. Coat.*, 45 (2002) 415.
13. H. Marchebois, S. Joiret, C. Savall, J. Bernard and S. Touzain, *Surf. Coat. Technol.*, 157 (2002) 151.
14. A. Kalendová, D. Veselý, M. Kohl and J. Stejskal, *Prog. Org. Coat.*, 78 (2015) 1.
15. A. Gergely, Z. Pászti, J. Mihály, E. Drotár and T. Török, *Prog. Org. Coat.*, 78 (2015) 437.
16. A. Gergely, Z. Pászti, J. Mihály, E. Drotár and T. Török, *Prog. Org. Coat.*, 77 (2014) 412.
17. B. Ramezanzadeh, S.Y. Arman and M. Mehdipour, *J.Coat. Technol. Res.*, 11 (2014) 727.
18. F.T. Shirehjini, I. Danaee, H. Eskandari and D. Zarei, *J.Coat. Technol. Res.*, 32 (2016) 1152.
19. Y. Su, V.G. Kravets, S.L. Wong, J. Waters, A.K. Geim and R.R. Nair, *Nat. Commun.*, 5 (2014) 4843.
20. C. Rao, K. Biswas, K. Subrahmanyam and A. Govindaraj, *J. Mater. Chem.*, 19 (2009) 2457.
21. R. Ding and W. Li, *J. Alloy. Compd.*, 764 (2018) 1039.
22. R. Ding, Y. Zheng, H. Yu, W. Li, X. Wang and T. Gui, *J. Alloy. Compd.*, 748 (2018) 481.
23. R. Ding, X. Wang, J. Jiang, T. Gui and W. Li, *J. Mater. Eng. Perform.*, 26 (2017) 3319.
24. X. Wang, S. Chen, R. Ding, N. Zhou, Y. Zheng, H.-b. Yu, B.-j. Li, T.-j. Gui and W.-h. Li, *Inter. J. Electrochem. Sci.*, 14 (2019) 3553.
25. B. Ramezanzadeh, M.H.M. Moghadam, N. Shohani and M. Mahdavian, *Chem. Eng. J.*, 320 (2017) 363.
26. H. Hayatdavoudi and M. Rahsepar, *J. Alloy. Compd.*, 727 (2017) 1148.
27. M. Mo, W. Zhao, Z. Chen, Q. Yu, Z. Zeng, X. Wu and Q. Xue, *RSC Adv.*, 5 (2015) 56486.
28. S. Chen, J. Zhu, X. Wu, Q. Han and X. Wang, *ACS Nano*, 4 (2010) 2822.
29. Z. Chen and L. Gao, Develop. *App. Mater.*, 30 (2015) 19.
30. S. Real, A. Elias, J. Vilche, C. Gervasi and A.D. Sarli, *Electrochim. Acta*, 38 (1993) 2029.
31. B.Y. Chang and S.M. Park, *Annu. Rev. Anal. Chem.*, 3 (2010) 207.
32. J.T. Zhang, J.M. Hu, J.Q. Zhang and C.N. Cao, *Prog. Org. Coat.*, 51 (2004) 145.
33. Y. Huang, H. Shih and F. Mansfeld, *Mater. corr.*, 61 (2010) 302.
34. M.S. Harding, B. Tribollet, V. Vivier and M.E. Orazem, *J. Electrochem. Soc.*, 164 (2017) 3418.
35. C. Hsu and F. Mansfeld, *Corr.*, 57 (2001) 747.

36. C. Abreu, M. Izquierdo, M. Keddam, X. Novoa and H. Takenouti, *Electrochim. Acta*, 41 (1996) 2405.
37. H. Marchebois, M. Keddam, C. Savall, J. Bernard and S. Touzain, *Electrochim. Acta*, 49 (2004) 1719.
38. J. Zhang, J. Hu, J. Zhang and C. Cao, *Prog. Org. Coat.*, 49 (2004) 293.
39. J. Hu, J. Zhang and C. Cao, *Prog. Org. Coat.*, 46 (2003) 273.
40. J. Liu, X.B. Li, J. Wang, T.Y. Luo and X.M. Wang, *Prog. Org. Coat.*, 76 (2013) 1075.